

Asymmetric Wave Propagation Through Nonlinear PT-symmetric Oligomers

J. D'Ambroise

Department of Mathematics, Bard College, Annandale, NY 12504

P.G. Kevrekidis

Department of Mathematics and Statistics, University of Massachusetts, Amherst, Massachusetts 01003-4515, USA

S. Lepri

*CNR-Consiglio Nazionale delle Ricerche, Istituto dei Sistemi Complessi,
via Madonna del piano 10, I-50019 Sesto Fiorentino, Italy*

In the present paper, we consider nonlinear PT-symmetric dimers and trimers (more generally, oligomers) embedded within a linear Schrödinger lattice. We examine the stationary states of such chains in the form of plane waves, and analytically compute their reflection and transmission coefficients through the nonlinear PT symmetric oligomer, as well as the corresponding rectification factors which clearly illustrate the asymmetry between left and right propagation in such systems. We examine not only the existence but also the dynamical stability of the plane wave states and interestingly find them to be generically unstable. Lastly, we generalize our numerical considerations to the more physically relevant case of Gaussian initial wavepackets and confirm that the asymmetry in the transmission properties persists in the case of such wavepackets, as well.

INTRODUCTION

Over the last fifteen years, and ever since its original proposal by Bender and co-workers [1], the study of PT-symmetric Hamiltonian systems has become a focal point for numerous investigations at the interface between theoretical physics and applied mathematics. The fundamental appeal of such systems is that they respect key physical symmetries, namely the Parity (P) and Time-reversal (T) (but not necessarily the stronger constraint of the Hamiltonian being Hermitian), thus providing an intriguing alternative set of Hamiltonians with potentially real eigenvalues. In the context that we will examine below and for standard Schrödinger Hamiltonians with a complex potential V , the above constraints of PT symmetry amount to the potential satisfying the condition $V(x) = V^*(-x)$.

While this field commenced as, arguably, a mathematical curiosity associated with the foundations of quantum mechanics, a major development from the point of view of applications arose recently. This was due to Christodoulides and co-workers [2] who realized that nonlinear optics (and the synthetic systems that can be engineered therein) may present a fertile playground for the experimental implementation of such PT-symmetric dynamics. Furthermore, the added feature of nonlinearity typically present in such settings initiated the consideration of the effects of such PT-symmetric potentials on the nonlinear waves (such as bright or gap solitons) that may arise therein. Subsequently, the first realizations of PT-symmetry arose both in the nonlinear optics of waveguide couplers (i.e., either two waveguides with and without loss [3] – the so-called passive PT– or in the more “standard” case of one waveguide with gain and one with loss [4]) and also in that of electronic analogs thereof [5]. This progress and the perspectives that it enables towards future developments have, in turn, fueled a considerable volume of further theoretical studies both within the realm of linear PT-symmetric potentials [6–14] and even in that of so-called nonlinear PT-symmetric potentials (i.e., where the PT-symmetric prefactor appears in front of the nonlinear term) [15–17].

Another theme that has received considerable attention recently concerns the study of asymmetric (i.e., non-reciprocal) wave propagation in the context of various applications. Among the first examples discussed in the literature is the asymmetric phonon transmission through a nonlinear interface layer between two very dissimilar crystals [18]. Later on, the theoretical proposition of a thermal diode [19] induced relevant experimental realizations in [20]; similarly, an optical diode [21] was theoretically proposed [22] and experimentally realized [23]. More recently similar proposals have been presented in left-handed metamaterials [24] and have, in fact, been experimentally realized by different groups also in the context of acoustic waves in granular systems [25, 26]. In fact, recently this theme has been examined in the context of PT periodic structures which have been shown [11] to act as unidirectional invisible media (at least for sufficiently small extents of the periodic structure [27]) with transmission coefficients and phases identical to the ones in the absence of the PT-structure.

In the present work, we adopt a different perspective to that of these recent works and in fact one closer to the considerations of [28]. The latter work considered a linear lattice in the presence of a set of N (embedded within the linear lattice) nonlinear elements. It was then shown that an asymmetry within the linear or nonlinear (still Hamiltonian though) properties of these elements would lead to an asymmetry of the relevant transmission of a plane wave through the chain. This was then extended to the more physically realistic case of a Gaussian wavepacket whose asymmetry was examined between incidence (on the asymmetric nonlinear region) from the left and from the right.

Here, we consider these notions of asymmetric wave propagation but for PT-symmetric oligomers (namely dimers,

trimers, quadrimers, etc.; see also the earlier study of such oligomers [12] which has motivated further recent studies such as the examination of quadrimers in [29]). In particular, we examine both the similarities and the differences with the above picture. In particular, we start our considerations by examining the transmission of plane waves through the chain. For such states, we analytically identify their reflection and transmission coefficients and obtain the corresponding transmittivity. We find some fundamental differences here in that such a quantity may exceed unity due to the presence of gain. Furthermore, we identify another fundamental difference in that beyond a particular gain strength a supercritical amount of “mass” may be collected at the gain site that may in turn lead to indefinite growth on this site. Nevertheless, for PT-coefficient strengths which yield meaningful transmittivities, a rectification factor is computed and clearly evidences the asymmetry between left and right propagation. Another aspect of the relevant plane wave solutions that we clarify concerns their generic dynamical instability, which we quantify and illustrate the (again, focusing) dynamical manifestation thereof. Lastly, we generalize our considerations (numerically) to the prototypical physically relevant case of an incident Gaussian wavepacket. We showcase that in that case as well, the transmission result differs between left and right such wavepackets impinging on the nonlinear PT-symmetric lattice region.

Our presentation is structured as follows. In section II, we will give an overview of the relevant theory (some of the pertinent, more cumbersome details are relegated to an appendix). In section III, the analytical results are illustrated through numerical computations of both the transmittivities and rectification factors (both for the plane wave structures and for the Gaussian wavepackets) and of the existence, spectral stability and nonlinear dynamics of the plane waves. Finally, in section IV, we summarize our findings and present some directions for future studies.

THEORETICAL ANALYSIS

Stationary DNLS

Starting our considerations with the existence of stationary solutions of the chain of interest, we examine the set of algebraic equations

$$\omega\psi_n = V_n\psi_n - \psi_{n+1} - \psi_{n-1} + \alpha_n|\psi_n|^2\psi_n \quad (1)$$

on a one-dimensional lattice for $\psi_n \in \mathbb{C}$ and $\omega \in \mathbb{R}$. The parameters $V_n \in \mathbb{C}$ and $\alpha_n \in \mathbb{R}$ are zero everywhere except for $1 \leq n \leq N$ so that the wave propagates freely outside of a finite region containing the nonlinearity and the (intended to be PT-symmetric, hence generally complex) linear potential. Rearranging (1) one obtains the so-called backward transfer map

$$\psi_{n-1} = -\psi_{n+1} + (V_n - \omega + \alpha_n|\psi_n|^2)\psi_n \quad (2)$$

from which solutions to (1) can be constructed from knowledge of ψ_n at two nodes.

The class of solutions whose (transmission and reflection) properties will be theoretically analyzed consists of plane waves of the form

$$\psi_n = \begin{cases} R_0 e^{ik_0 n} + R e^{-ik_0 n} & n \leq 1 \\ T e^{ik_0 n} & n \geq N \end{cases} \quad (3)$$

with $R_0, R, T \in \mathbb{C}$ representing the incident, reflected and transmitted amplitudes, respectively. Note that outside of the nonlinear region, for $n < 1$ and $n > N$, (3) satisfies (1) for any R_0, R and T if $\omega = -2\cos(k_0)$. Also directly from (3) [as applied to sites with $n = 0$ and $n = 1$], we have

$$R_0 = \frac{e^{-ik_0}\psi_0 - \psi_1}{e^{-ik_0} - e^{ik_0}} \quad \text{and} \quad R = \frac{e^{ik_0}\psi_0 - \psi_1}{e^{ik_0} - e^{-ik_0}}. \quad (4)$$

Thus, for any fixed values of k_0 and T , ψ_0 and ψ_1 can be calculated by applying (2) iteratively starting with $\psi_N = T e^{ik_0 N}$ and $\psi_{N+1} = T e^{ik_0(N+1)}$ from (3). Then, (4) gives the appropriate values of R_0 and R so that (1) is satisfied at all nodes.

For convenience we write the backward transfer map with $n = N - l + 1$ and in terms of Ψ_n for $\psi_n \stackrel{\text{def.}}{=} T e^{ik_0 N} \Psi_n$. This gives

$$\Psi_{N-l} = -\Psi_{N-l+2} + \delta_{N-l+1} \Psi_{N-l+1} \quad (5)$$

for $\delta_j \stackrel{\text{def.}}{=} V_j - \omega + \alpha_j |T|^2 |\Psi_j|^2$. For example, applying (5) with $N = 2$ and $\Psi_3 = e^{ik_0}$, $\Psi_2 = 1$ gives

$$\begin{aligned} \delta_2 &= V_2 - \omega + \alpha_2 |T|^2 \\ \Psi_1 &= -e^{ik_0} + \delta_2 \\ \delta_1 &= V_1 - \omega + \alpha_1 |T|^2 |\delta_2 - e^{ik_0}|^2 \\ \Psi_0 &= -1 + \delta_1 (\delta_2 - e^{ik_0}). \end{aligned} \quad (6)$$

Finally by (4) and (6) we have

$$R_0 = \frac{Te^{ik_0}}{e^{-ik_0} - e^{ik_0}} (-1 + (\delta_1 - e^{ik_0})(\delta_2 - e^{ik_0})) \quad (7)$$

and the corresponding transmission coefficient $t \stackrel{\text{def}}{=} |T|^2/|R_0|^2$ is then

$$t = \left| \frac{e^{ik_0} - e^{-ik_0}}{1 + (\delta_1 - e^{ik_0})(e^{ik_0} - \delta_2)} \right|^2. \quad (8)$$

In the linear case ($\alpha_1 = \alpha_2 = 0$), it is immediately seen that t is the same for waves coming from the left or right side, independently of V_n , as prescribed by the reciprocity theorem [28, 30].

It should be noted here that although the relevant calculation was presented for $N = 2$, it can be performed for arbitrary values of N (naturally, the complexity of the intermediate steps is increased, the higher the value of N). For reasons of clarity of exposition but also of completeness, the relevant presentation has been given in the Appendix. We should also note that in comparison to the earlier work of [28], there are fundamental similarities in the approach but also important differences in the nature of the results since our quantities δ_i (corresponding to the ν and δ , respectively in [28]) are now, in principle, complex rather than purely real. Let us also indicate here that to quantify asymmetric propagation we will use the definition of a rectification factor f in the form:

$$f = \frac{t(k_0, T) - t(-k_0, T)}{t(k_0, T) + t(-k_0, T)}, \quad (9)$$

whose non-vanishing values in the range $[-1, 1]$ are measures of the asymmetry of transmission in the system (symmetric transmission is tantamount to $f = 0$).

Time Propagation

We also briefly touch upon the tools that we will use towards the consideration of the dynamical evolution phenomena within our nonlinear Schrödinger type chains

$$i\dot{\phi}_n(t) - V_n\phi_n(t) + \phi_{n+1}(t) + \phi_{n-1}(t) = \alpha_n|\phi_n(t)|^2\phi_n(t). \quad (10)$$

In particular, in addition to direct numerical integration of Eq. (10), so as to monitor the dynamical evolution of the solutions, we will use a spectral stability analysis of stationary states (of the form $\psi_n e^{-i\omega t}$ discussed in the previous section) according to

$$\phi_n(t) = \rho_n(t) + \epsilon p_n(t). \quad (11)$$

Here, $\rho_n(t) = \psi_n e^{-i\omega t}$ and $p_n(t) = e^{-i\omega t} (a_n e^{i\nu t} + b_n e^{-i\nu^* t})$ for $\omega \in \mathbb{R}$ and $a_n, b_n, \nu \in \mathbb{C}$. ρ_n is assumed to be a standing wave solution of (10) so that the resulting order- ϵ equation for $p_n(t)$ is

$$i\dot{p}_n - V_n p_n + p_{n+1} + p_{n-1} + \omega p_n = \alpha_n (2p_n |\rho_n|^2 + \rho_n^2 p_n^*). \quad (12)$$

The ensuing linear stability equations will yield the eigen-problem of the form:

$$\nu \begin{pmatrix} a_n \\ b_n^* \end{pmatrix} = \begin{pmatrix} F_1 & F_2 \\ F_3 & F_4 \end{pmatrix} \begin{pmatrix} a_n \\ b_n^* \end{pmatrix} \quad (13)$$

for

$$\begin{aligned} F_1 &= \text{diag}(\omega - V_n - 2\alpha_n |\psi_n|^2) + G \\ F_2 &= \text{diag}(-\alpha_n \psi_n^2) \\ F_3 &= \text{diag}(\alpha_n (\psi_n^*)^2) \\ F_4 &= \text{diag}(-\omega + V_n^* + 2\alpha_n |\psi_n|^2) - G, \end{aligned} \quad (14)$$

where G is a sparse matrix with ones on the superdiagonal and the subdiagonal. Note that in (13) it is now convenient to think of a_n and b_n as column vectors. Given a stationary solution ρ_n and values of V_n, α_n which encode the nonlinearity for $1 \leq n \leq N$, one then calculates the eigenvalues ν in (13). If ν has a nonzero imaginary part this indicates that the perturbed solution $\phi_n(t)$ is unstable, as is easily seen by the form of $p_n(t)$ specified above. In practice, one diagonalizes a finite truncation of the matrix in (13), checking that the relevant eigenvalues are not affected by the truncation error.

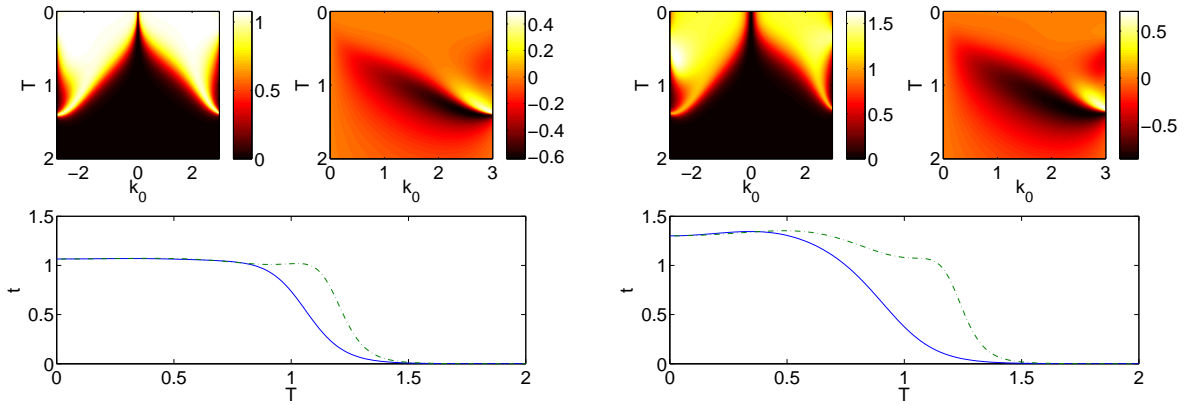


FIG. 1: The figure presents the case of a PT-symmetric dimer with $N = 2$, $\alpha_{1,2} = 1$, while $V_1 = i\gamma$ and $V_2 = -i\gamma$. The left set of panels corresponds to the case of $\gamma = 0.25$, while the right set of panels to the case of $\gamma = 0.5$. Each set contains a contour plot of $t(k_0, T)$ (top left), a contour plot of $f(k_0, T)$ and a typical example of the dependence of t for $k_0 = 2$ (solid lines) and $k_0 = -2$ (dashed lines), so as to illustrate the asymmetry between the propagation for left and right incident waves.

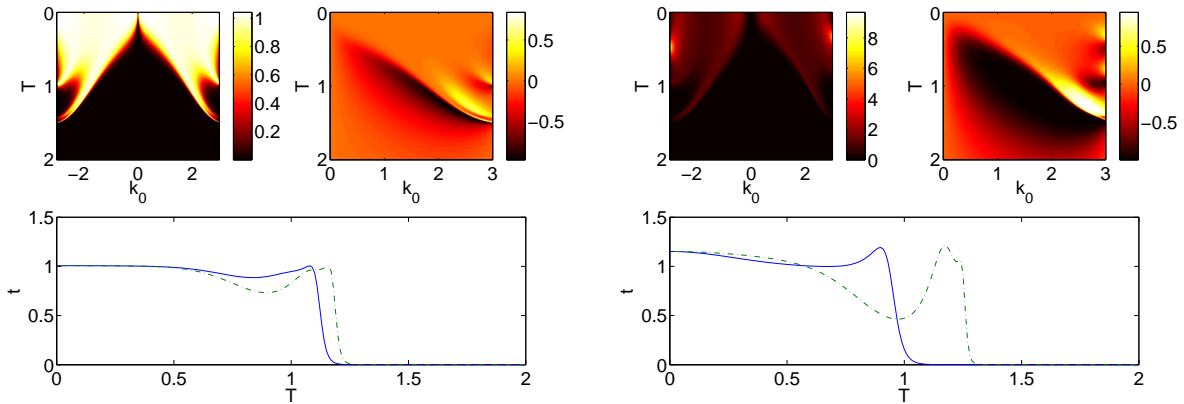


FIG. 2: Same as the figure above but now for the trimer case of $N = 3$, $\alpha_{1,2,3} = 1$, while $V_1 = i\gamma$, $V_2 = 0$ and $V_3 = -i\gamma$. The specific values of γ for the panels given are $\gamma = 0.1$ and $\gamma = 0.45$.

NUMERICAL COMPUTATIONS

We now turn to computations in order to quantify the above theoretical results (as well as to extend beyond the range of what is analytically tractable).

We start with the consideration of the transmittivity $t(k_0, T)$ and of the rectification factor $f(k_0, T)$ which are given for the case of the PT-symmetric dimer in Fig. 1 and for the PT-symmetric trimer in Fig. 2. The nonlinearity is uniform in both cases, but the linear potential is $V_1 = -V_2 = i\gamma$ in the former, while it is $V_1 = -V_3 = i\gamma$ and $V_2 = 0$ in the latter. In both cases, a typical example of the transmittivity dependence for $k_0 = 2$ and $k_0 = -2$ is shown in the bottom panel of the figures. The asymmetry which is present in the top left panels between positive and negative values of k_0 and which is further quantified in the rectification factor of the top right panels clearly makes the case for the asymmetric wave propagation in these PT-symmetric oligomers. Although the values used here are below the PT transition of the underlying linear oligomer system, we have ensured that the relevant characteristic behavior (and presented asymmetries) exist both below and above that transition. However, as can also be inferred from the figures, the higher the value of PT-symmetric parameter γ , the stronger the manifestations of the asymmetric propagation of the waves. Another relevant observation to make here is that although the rectification factor is by construction bounded within $[-1, 1]$, the transmittivity is not bounded by unity (contrary to what is the case in the Hamiltonian example of [28]). Hence, we can observe that in all the examples of t shown the relevant factor may exceed unity thus illustrating the existence of gain in the system.

We now wish to touch upon one important aspect of the extended solutions ψ_n , identified in the form of Eq. (3). Interestingly, a detailed examination of the stability properties of these solutions in fact reveals that they are generi-

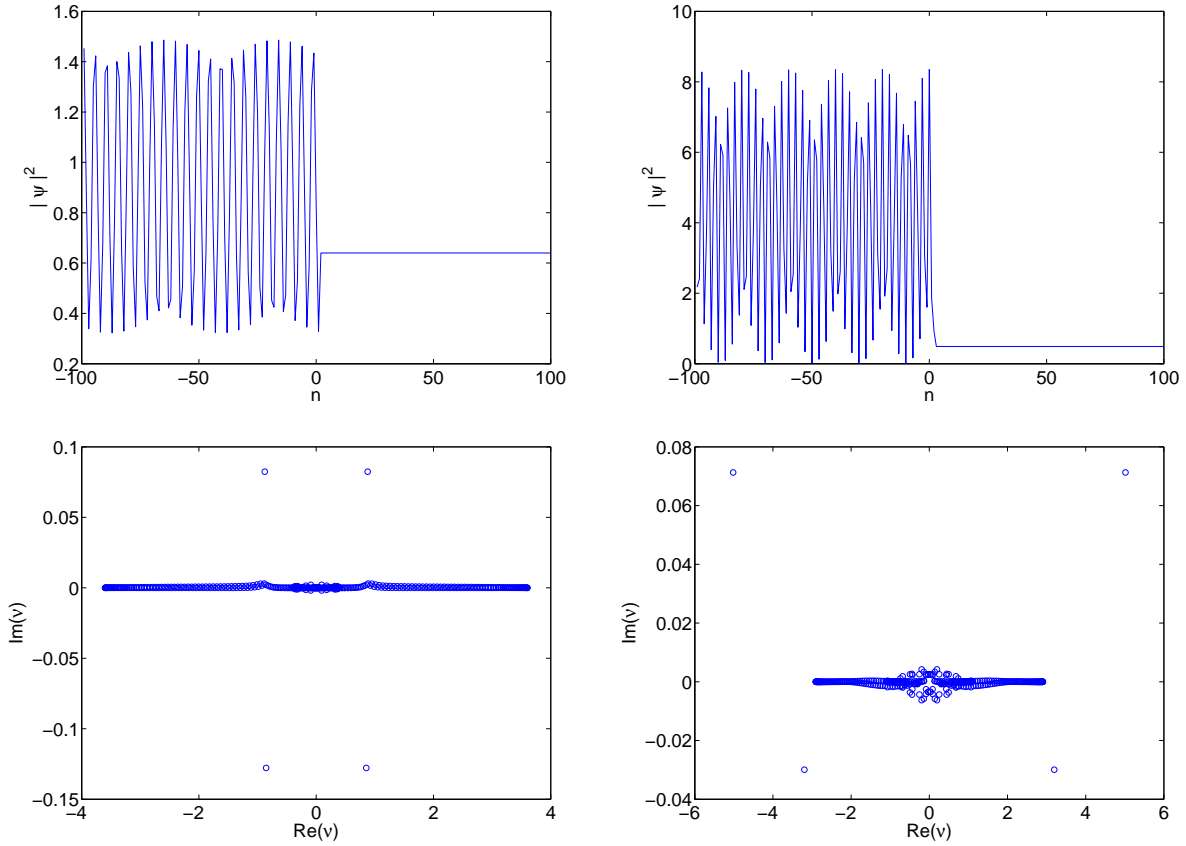


FIG. 3: The bottom panels show eigenvalues of the linearization of the example solutions shown in the top panel. In the PT-symmetric dimer (left), the parameters are $N = 2$ with $k_0 = 2.5$, $T = 0.8$, $\gamma = 0.1$, while in the PT-symmetric trimer (right), they are: $N = 3$ with $k_0 = 1.1$, $T = 0.7$, $\gamma = 0.1$.

cally unstable. A typical example of the corresponding spectral plane ($\text{Re}(\nu), \text{Im}(\nu)$) of eigenfrequencies $\nu = \text{Re}(\nu) + i\text{Im}(\nu)$ is shown for an example of the dimer and a corresponding one of the trimer in Fig. 3. In fact, our computations indicate that this feature persists in the Hamiltonian variant of the model of Ref. [28] (although a more detailed examination of the latter is of interest in its own right). The dynamical instability observed via the presence of imaginary eigenfrequencies in the spectral plane of the PT-symmetric oligomers is corroborated by direct numerical simulations in Fig. 4. Here, we initialize the lattice with the solutions that were shown to be unstable via the spectral analysis of Fig. 3, to which a normally distributed small amplitude random perturbation has been superposed. The manifestation of the instability once again clearly underscores the role of the gain in the system. In particular, the dynamics reveals the tendency of the site which has gain to acquire a super-critical “mass” (or density), which subsequently grows exponentially well beyond the density of the linear background (or of the sites with loss).

Given the above considerations and also the lesser physical relevance of exciting an initial condition of the form of Eq. (3) in an optical setting (which would be the prototypical potential realization of the considerations presented herein), we now turn to the examination of the dynamics of a more localized Gaussian wavepacket. The latter is assumed to be of the form:

$$\psi_n = I e^{ik_0 n - (n - n_0)^2 / s^2}, \quad (15)$$

i.e., of amplitude I , centered at $n_0 \in \mathbb{Z}$, while its speed is controlled by the parameter k_0 which assumes values in the interval $-\pi \leq k_0 \leq \pi$ and s (chosen to assume the value 10 in what follows) is a parameter controlling the wavepacket width. It should be noted here that this aspect of our consideration is purely numerical (as it is not straightforward to obtain explicit analytical expressions for the transmission and reflection coefficients in this case). We thus evolve an incident wavepacket from the left or from the right and observe its propagation as illustrated in the space-time contour plots of Fig. 5. In what is shown below, we have performed the numerical computations for $I = 1$, but we have confirmed that the relevant phenomenology persists for a wide range of non-vanishing values of I (approaching the linear limit of $I \rightarrow 0$ approaches vanishing transmittivity differences, once again due to the principle of reciprocity).

The transmission coefficient in this case is defined as the fraction of the total sum of the squared modulus of the

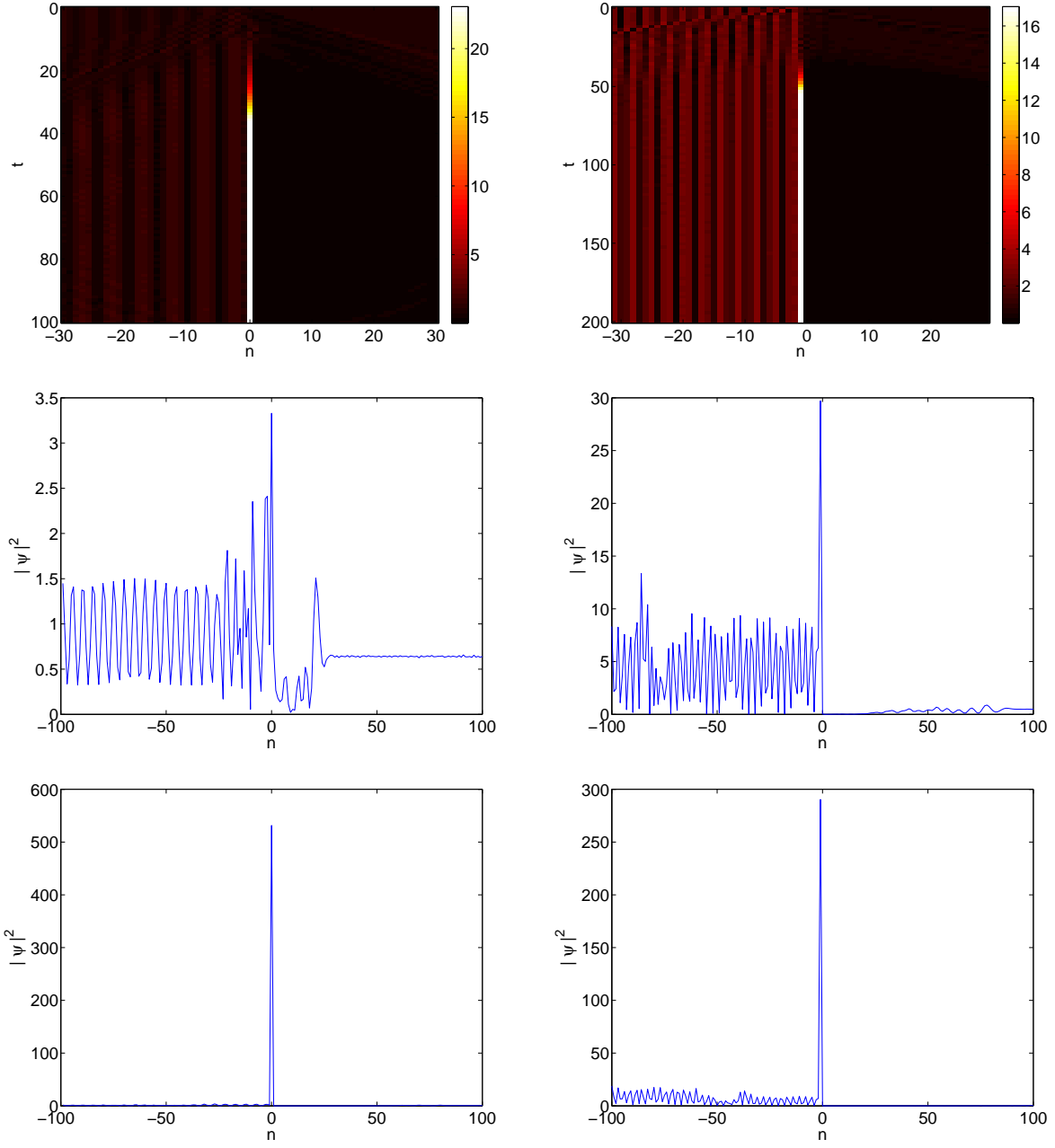


FIG. 4: The top panel shows the contour plot of the space n - time t evolution of $|\phi_n|$ for the solutions/parameters corresponding to the left and right, respectively, panels of Fig. 3. The rest of the panels show individual snapshots of the solution at $t = 10, 40$ (for the left panels of the dimer case) and at $t = 40, 80$ (for the right panels of the trimer case).

field across nodes that is transmitted to the right of the PT-symmetric oligomer after the Gaussian wavepacket passes over the relevant nodes. That is, we define $t_{k_0} = \sum_{n < 1} |\phi_n|^2 / \sum_n |\phi_n|^2$ for $k_0 < 0$ and $t_{k_0} = \sum_{n > N} |\phi_n|^2 / \sum_n |\phi_n|^2$ for $k_0 > 0$. We find that the transmittivity is greater for Gaussians approaching from the right and that the transmittivity difference is amplified as γ increases, see Figure 6 which presents the relevant rectifying factor. This can be qualitatively understood once again on the basis of the structure of the PT oligomer. The node that has gain (which is on the left) favors reflection for a wavepacket from the left, while it favors transmission for a wavepacket impinging from the right, hence ensuring that $t_{-k_0} > t_{k_0}$ in our setup. Interestingly, in this case of the Gaussian wavepacket as well, for a high enough value of γ the density accumulates and grows indefinitely at the nonlinear node that bears the gain. On the dimer with $k_0 = \pi/2$ this critical value is $\gamma \simeq 0.6531$, and with $k_0 = -\pi/2$ it is $\gamma \simeq 1.0890$. On the trimer with $k_0 = \pi/2$ the blowup occurs for $\gamma \simeq 0.6737$ and with $k_0 = -\pi/2$ the value is $\gamma \simeq 0.8043$. We note once again that these features are unique to the case of PT-symmetric oligomers through their gain-loss pattern and would be entirely absent in the earlier Hamiltonian installment of such chains in [28].

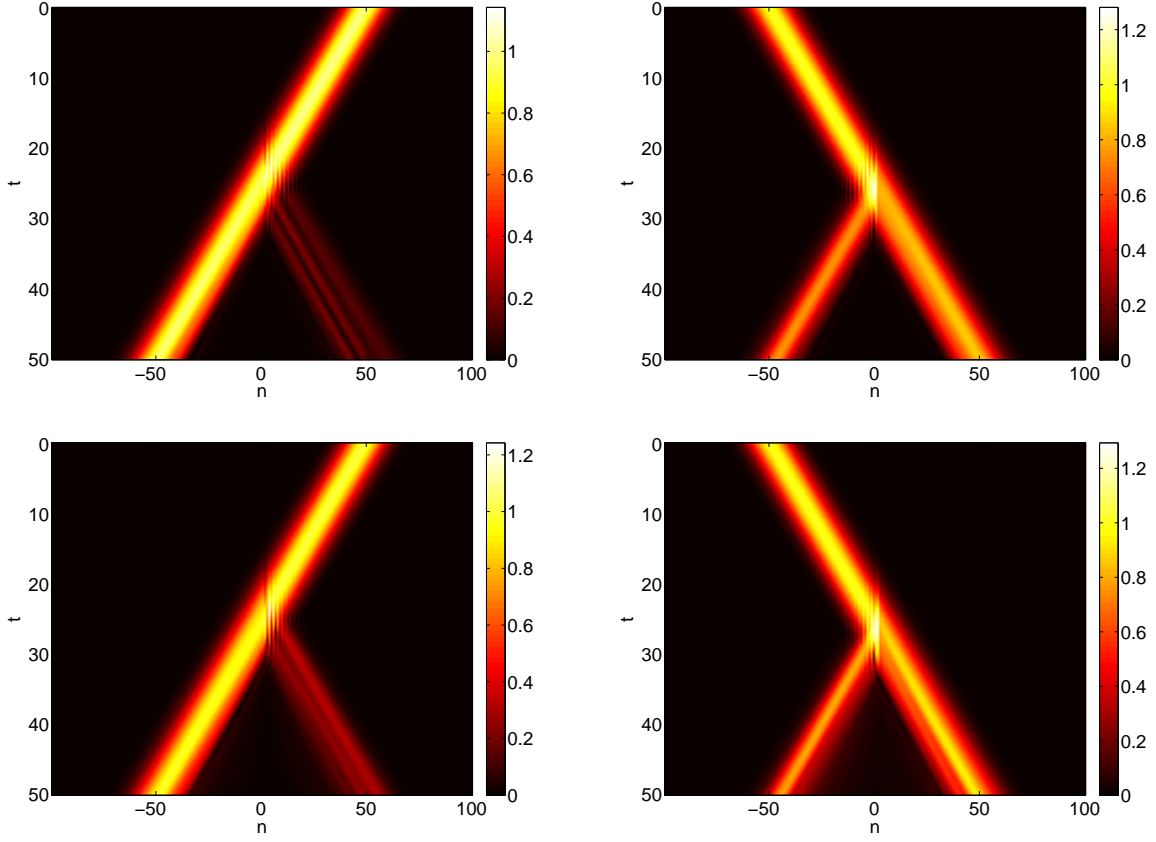


FIG. 5: The space-time contour plot of $|\phi_n(t)|^2$ is shown for left and right incidence on the PT-symmetric dimer (top panels) and on the PT-symmetric trimer (bottom panels). Top: dimer, $N = 2$ with $n_0 = -50$, $s = 10$, $k_0 = -\pi/2$ (left) and $k_0 = \pi/2$ (right); Bottom: trimer, $N = 3$ with $n_0 = -50$, $s = 10$, $k_0 = -\pi/2$ (left) and $k_0 = \pi/2$ (right),

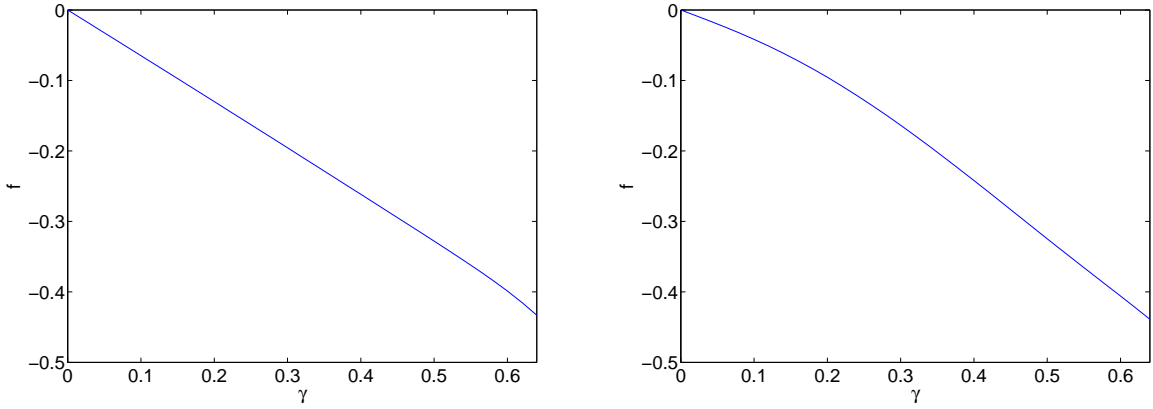


FIG. 6: Rectifying factor for the incidence of a Gaussian wavepacket on the PT-symmetric dimer and trimer. Left: dimer, $N = 2$ with $k_0 = \pi/2$, $n_0 = -50$, $s = 10$; Right: trimer, $N = 3$ with $k_0 = \pi/2$, $n_0 = -50$, $s = 10$.

CONCLUSIONS

In the present work, we considered a lattice setting where embedded in a linear Schrödinger chain was a nonlinear PT-symmetric oligomer, typically a dimer or a trimer. Our analytical considerations were focused around plane waves enabling us to analytically compute both the transmittivity and the rectification factor between left- and right-propagating such waves. These features amply evidenced the asymmetric nature of the propagation and even illustrated features particular to the gain-loss systems, such as the existence of over-unity transmittivities. On

the other hand, we also considered the spectral stability of such states revealing their generic instability that was monitored and shown dynamically to lead to mass focusing on a single (gain) node of the lattice. This (as well as the more straightforward realization of a localized excitation in such lattices), in turn, led us to the consideration of the asymmetry of propagation of a Gaussian wavepacket which we numerically quantified. Here, too, however the interesting phenomenon of the potential trapping of mass in a particular site with gain and the subsequent indefinite growth thereof were observed and quantified.

These results suggest numerous interesting investigations for future work. It would be relevant to attempt to theoretically quantify transmittivities and reflectivities of a Gaussian wavepacket perhaps through a judicious variational ansatz or some similar method that appropriately reduces the degrees of freedom, while taking into consideration both the complex PT-oligomer dynamics and the generic existence of a reflecting and a transmitting wavepacket. On the other hand, it would be particularly interesting to generalize the relevant considerations to higher dimensional settings and examine how incident waves from different directions may affect the transmittivity of different forms of two-dimensional PT-symmetric oligomers (in the simplest genuinely two dimensional case, PT-symmetric squares). These themes will be considered in future studies.

PGK gratefully acknowledges support from the US-NSF through grants DMS-0806762 and CMMI-1000337 and from the Alexander von Humboldt Foundation, the Alexander S. Onassis Public Benefit Foundation (through grant RZG 003/2010-2011) and from the Binational Science Foundation (through grant 2010239). SL acknowledges support from the Miur PRIN 2008 project *Efficienza delle macchine termoelettriche: un approccio microscopico*.

-
- [1] C.M. Bender and S. Boettcher, Phys. Rev. Lett. **80**, 5243 (1998); C.M. Bender, S. Boettcher and P.N. Meisinger, J. Math. Phys. **40**, 2201 (1999)
 - [2] Z.H. Musslimani, K.G. Makris, R. El-Ganainy and D.N. Christodoulides, Phys. Rev. Lett. **100**, 030402 (2008); K.G. Makris, R. El-Ganainy, D.N. Christodoulides and Z.H. Musslimani, Phys. Rev. A **81**, 063807 (2010).
 - [3] A. Guo, G. J. Salamo, D. Duchesne, R. Morandotti, M. Volatier-Ravat, V. Aimez, G. A. Siviloglou and D. N. Christodoulides, Phys. Rev. Lett. **103**, 093902 (2009).
 - [4] C.E. Rüter, K.G. Makris, R. El-Ganainy, D.N. Christodoulides, M. Segev, D. Kip, Nature Phys. **6**, 192 (2010).
 - [5] J. Schindler, A. Li, M.C. Zheng, F.M. Ellis and T. Kottos, Phys. Rev. A **84**, 040101 (2011).
 - [6] H. Ramezani, T. Kottos, R. El-Ganainy and D.N. Christodoulides, Phys. Rev. A **82**, 043803 (2010).
 - [7] A.A. Sukhorukov, Z. Xu and Yu.S. Kivshar, Phys. Rev. A **82**, 043818 (2010).
 - [8] M.C. Zheng, D.N. Christodoulides, R. Fleischmann and T. Kottos, Phys. Rev. A **82**, 010103(R) (2010).
 - [9] E.M. Graefe, H.J. Korsch and A.E. Niederle, Phys. Rev. Lett. **101**, 150408 (2008).
 - [10] E.M. Graefe, H.J. Korsch and A.E. Niederle, Phys. Rev. A **82**, 013629 (2010).
 - [11] Z. Lin, H. Ramezani, T. Eichelkraut, T. Kottos, H. Cao and D.N. Christodoulides, Phys. Rev. Lett. **106**, 213901 (2011).
 - [12] K. Li and P. G. Kevrekidis Phys. Rev. E **83**, 066608 (2011)
 - [13] S.V. Dmitriev, S.V. Suchkov, A.A. Sukhorukov, and Yu.S. Kivshar, Phys. Rev. A **84**, 013833 (2011)
 - [14] S.V. Suchkov, B.A. Malomed, S.V. Dmitriev and Yu.S. Kivshar, Phys. Rev. E **84**, 046609 (2011).
 - [15] A.E. Miroshnichenko, B.A. Malomed, and Yu.S. Kivshar Phys. Rev. A **84**, 012123 (2011).
 - [16] F.Kh. Abdullaev, Y.V. Kartashov, V.V. Konotop and D.A. Zezyulin, Phys. Rev. A **83**, 041805 (2011)
 - [17] D. A. Zezyulin, Y. V. Kartashov, V. V. Konotop, arXiv:1111.0898.
 - [18] Yu. A. Kosevich, Phys. Rev. B, **52**, 1017 (1995).
 - [19] M. Terraneo, M. Peyrard, and G. Casati, Phys. Rev. Lett. **88**, 094302 (2002).
 - [20] C.W. Chang, D. Okawa, A. Majumdar, and A. Zettl, Science **314**, 1121 (2006); W. Kobayashi, Y. Teraoka, and I. Terasaki, Appl. Phys. Lett. **95**, 171905 (2009).
 - [21] M. Scalora, J. P. Dowling, C. M. Bowden, and M. J. Bloemer, J. Appl. Phys. **76**, 2023 (1994); M. D. Tocci, M. J. Bloemer, M. Scalora, J. P. Dowling, and C. M. Bowden, Appl. Phys. Lett. **66**, 2324 (1995).
 - [22] V.V. Konotop and V. Kuzmiak, Phys. Rev. B **66**, 235208 (2002). B. Liang, B. Yuan and J.C. Cheng, Phys. Rev. Lett. **103**, 104301 (2009).
 - [23] K. Gallo, G. Assanto, K. Parameswaran and M. Fejer, Appl. Phys. Lett. **79**, 314 (2001).
 - [24] M.W. Feise, I.V. Shadrivov and Y.S. Kivshar, Phys. Rev. E **71**, 037602 (2005).
 - [25] N. Boechler, G. Theoharis and C. Daraio, Nature Materials **10**, 665 (2011).
 - [26] B. Liang, B. Yuan and J.C. Cheng, Phys. Rev. Lett. **103**, 104301 (2009); B. Liang, X.S. Guo, J. Tu, D. Zhang and J.C. Cheng, Nature Mater. **9**, 989992 (2010).
 - [27] S. Longhi, J. Phys. A. **44**, 485302 (2011).
 - [28] S. Lepri and G. Casati, Phys. Rev. Lett. **106**, 164101 (2011).
 - [29] D. A. Zezyulin, V. V. Konotop, arXiv:1202.3652.
 - [30] B.Lindquist, Phys. Rev. E **63**, 56605 (2001).

Appendix

For the record we show five iterations of (5) starting from $\Psi_{N+1} = e^{ik}$ and $\Psi_N = 1$:

$$\begin{aligned}
\delta_N &= V_N - \omega + \alpha_N |T|^2 \\
\Psi_{N-1} &= -\Psi_{N+1} + \delta_N \Psi_N \quad (l=1) \\
&= -e^{ik} + \delta_N \\
\delta_{N-1} &= V_{N-1} - \omega + \alpha_{N-1} |T|^2 |\delta_N - e^{ik}|^2 \\
\Psi_{N-2} &= -\Psi_N + \delta_{N-1} \Psi_{N-1} \quad (l=2) \\
&= -1 + \delta_{N-1} (\delta_N - e^{ik}) \\
\delta_{N-2} &= V_{N-2} - \omega + \alpha_{N-2} |T|^2 |1 + \delta_{N-1} (e^{ik} - \delta_N)|^2 \\
\Psi_{N-3} &= -\Psi_{N-1} + \delta_{N-2} \Psi_{N-2} \quad (l=3) \\
&= e^{ik} - \delta_N + \delta_{N-2} (-1 + \delta_{N-1} (\delta_N - e^{ik})) \\
&= -\delta_{N-2} + (e^{ik} - \delta_N) (1 - \delta_{N-2} \delta_{N-1}) \\
\delta_{N-3} &= V_{N-3} - \omega + \alpha_{N-3} |T|^2 |\delta_{N-2} + (\delta_N - e^{ik}) (1 - \delta_{N-2} \delta_{N-1})|^2 \\
\Psi_{N-4} &= -\Psi_{N-2} + \delta_{N-3} \Psi_{N-3} \quad (l=4) \\
&= 1 + \delta_{N-1} (e^{ik} - \delta_N) + \delta_{N-3} (-\delta_{N-2} + (e^{ik} - \delta_N) (1 - \delta_{N-2} \delta_{N-1})) \\
&= 1 - \delta_{N-3} \delta_{N-2} + (e^{ik} - \delta_N) (\delta_{N-1} + \delta_{N-3} (1 - \delta_{N-2} \delta_{N-1})) \\
\delta_{N-4} &= V_{N-4} - \omega + \alpha_{N-4} |T|^2 |1 - \delta_{N-3} \delta_{N-2} + (e^{ik} - \delta_N) (\delta_{N-1} + \delta_{N-3} (1 - \delta_{N-2} \delta_{N-1}))|^2 \\
\Psi_{N-5} &= -\Psi_{N-3} + \delta_{N-4} \Psi_{N-4} \quad (l=5) \\
&= \delta_{N-2} - (e^{ik} - \delta_N) (1 - \delta_{N-2} \delta_{N-1}) \\
&\quad + \delta_{N-4} (1 - \delta_{N-3} \delta_{N-2} + (e^{ik} - \delta_N) (\delta_{N-1} + \delta_{N-3} (1 - \delta_{N-2} \delta_{N-1}))) \\
&= \delta_{N-2} + \delta_{N-4} (1 - \delta_{N-3} \delta_{N-2}) \\
&\quad + (e^{ik} - \delta_N) (\delta_{N-4} \delta_{N-1} + (\delta_{N-4} \delta_{N-3} - 1) (1 - \delta_{N-2} \delta_{N-1})).
\end{aligned}$$

Notice that if we iterate N times we get δ 's equal to $-\omega$ since $V = \alpha = 0$ for these nodes. Then R_0 can be calculated from (4) in terms of appropriate δ 's.

For $N = 3$, the algorithm gives a transmission coefficient

$$t = \left| \frac{e^{ik} - e^{-ik}}{e^{ik} - \delta_1 + (e^{ik} - \delta_3)(1 - \delta_2(\delta_1 - e^{ik}))} \right|^2 \quad (16)$$

for

$$\begin{aligned}
\delta_3 &= V_3 - \omega + \alpha_3 |T|^2 \\
\delta_2 &= V_2 - \omega + \alpha_2 |T|^2 |\delta_3 - e^{ik}|^2 \\
\delta_1 &= V_1 - \omega + \alpha_1 |T|^2 |1 + \delta_2 (e^{ik} - \delta_3)|^2.
\end{aligned} \quad (17)$$

For $N = 4$ we obtain

$$t = \left| \frac{e^{ik} - e^{-ik}}{1 + \delta_2 (e^{ik} - \delta_1) + (e^{ik} - \delta_4) (\delta_3 + (1 - \delta_2 \delta_3) (\delta_1 - e^{ik}))} \right|^2 \quad (18)$$

for

$$\begin{aligned}
\delta_4 &= V_4 - \omega + \alpha_4 |T|^2 \\
\delta_3 &= V_3 - \omega + \alpha_3 |T|^2 |\delta_4 - e^{ik}|^2 \\
\delta_2 &= V_2 - \omega + \alpha_2 |T|^2 |1 + \delta_3 (e^{ik} - \delta_4)|^2 \\
\delta_1 &= V_1 - \omega + \alpha_1 |T|^2 |\delta_2 + (\delta_4 - e^{ik}) (1 - \delta_2 \delta_3)|^2.
\end{aligned} \quad (19)$$

For $N = 5$, we calculate

$$t = \left| \frac{e^{ik} - e^{-ik}}{\delta_3 + (\delta_1 - e^{ik}) (1 - \delta_2 \delta_3) + (e^{ik} - \delta_5) (\delta_4 (\delta_1 - e^{ik}) + (1 - \delta_3 \delta_4) (\delta_2 (\delta_1 - e^{ik}) - 1))} \right|^2 \quad (20)$$

for

$$\begin{aligned}
 \delta_5 &= V_5 - \omega + \alpha_5 |T|^2 \\
 \delta_4 &= V_4 - \omega + \alpha_4 |T|^2 |\delta_5 - e^{ik}|^2 \\
 \delta_3 &= V_3 - \omega + \alpha_3 |T|^2 |1 + \delta_4 (e^{ik} - \delta_5)|^2 \\
 \delta_2 &= V_2 - \omega + \alpha_2 |T|^2 |\delta_3 + (\delta_5 - e^{ik})(1 - \delta_3 \delta_4)|^2 \\
 \delta_1 &= V_1 - \omega + \alpha_1 |T|^2 \left| 1 - \delta_{N-3} \delta_{N-2} + (e^{ik} - \delta_N) (\delta_{N-1} + \delta_{N-3} (1 - \delta_{N-2} \delta_{N-1})) \right|^2.
 \end{aligned} \tag{21}$$